8th Biennial International Conference
& Exposition on Petroleum Geophysics

"HYDERABAD 2010"

P-37

# Tomographic imaging of the crust toward south of southern granulite terrain (SGT), India and its geodynamic implications

***Laxmidhar Behera****, *National Geophysical Research Institute (NGRI), Hyderbad*

***Summary***

*The crustal tomographic image is obtained toward south of SGT, India using deep seismic sounding data along 220 km N-S Vattalkundu-Kanyakumari profile acquired in 2005. The image depicts both subsurface structural and velocity heterogeneities along with numerous shear zones. The crust is thickest near Vattalkundu (44 km) and gradually thins toward Kanyakumari (36 km) with intracrustal undulations. The P-wave velocities for upper and lower crust range from 6.0-6.4 km/s and 6.7-7.1 km/s, respectively. The thick crust (>40 km) with high average velocity (>6.7 km/s) and high heat-flow (~58 mW/m$^2$) indicates complex tectonothermal evolution of the region. The Bouguer gravity data also show anomalous signatures near the Achankovil shear zone and the density model derived corroborates both preferred and tomographic velocity models. The high velocity (>6.9 km/s) and density (>2.9 g/cm$^3$) magmatic materials in the mid to lower crust is inferred as underplating. The thick (~10 km) lower crust with velocity 7.1 km/s and density 2.98 g/cm$^3$ show significant Moho upwarping due to mantle upwelling toward southern end. The presence of numerous shear zones with high-grade charnockite massifs in the upper crust exposed in several places reveal large scale exhumation of lower crustal rocks during the Pan-African rifting (~550 Ma). The final tectonic model derived show large compositional changes of rocks having horsts and grabens in the upper crust with exhumed granulites/charnockites forming a complex metamorphic province. The source region of exhumation lies at a depth of 20-30 km. The Moho configuration derived from tomography agrees well with preferred model.*

## Introduction

The southern granulite terrain (SGT) of India (Figure 1) is one of the three largest granulite provinces in the world like the Kapuskasing structural zone of Canada and the Arunta Block of Australia [Percival and Card, 1983]. The granulites present toward northern part of SGT are mainly composed of granite-greenstone (low-grade) terrain of Dharwar craton rich in tonalitic gneisses and granitic plutons and toward south of SGT are dominated by high-grade charnockite massifs rich in orthopyroxene. Some of these highland massifs reach to a maximum elevation of 2400m and also surrounded by deep valleys with numerous shear zones (Figure 1). The northern granulite block occupies area between Dharwar craton and Palghat-Cauvery shear (PCS) zone, which defines transition between low and high-grade granulitic terrains corresponding to late Archean metamorphic event (~2.5 Ga). The region between PCS and Achankovil shear (AKS) zone is the Madurai block (0.5 – 0.7 Ga) and the south of AKS is the Kerala khondalite block having sedimentary protolith comprises mainly khondalites and garnet-biotite-quarzofeldspathic gneisses with associated migmatite [Guru Rajesh and Chetty, 2006].

Most of the information about deep crustal structure is available toward north of SGT [Ramakrishna (Ed.), 2003]. The south of SGT has undergone a complex terrain accretion since mid-Archean and very little information is available till date about the poorly-defined tectonic boundaries at depth. To understand the complex geology and tectonic settings of the south of SGT, a 220 km-long N-S trending deep seismic sounding (DSS) profile was shot from Vattalkundu to Kanyakumari in 2005 [Prasad et al.,

*NGRI, Uppal Road, Hyderabad-500007, India, email: laxmidhar@ngri.res.in*

2006] traversing across the different shear zones (Figure 1). The seismic refraction/wide-angle reflection data was acquired for six wide-angle shots (explosives with charge size varying from 100-1200 kg in specially drilled holes depending upon the offset coverage) with the help of Radio Frequency Telemetry (RFT)-SN388 Sercel seismic data acquisition system. The shot (SP) spacing is ~40 km and geophone (vertical single component 4.5 Hz with ten geophone groups) spacing of ~100 m with continuous spreads at different offsets for each SP to acquire long offset data. Each spread consists of 180 channels to obtain dense data coverage. A preliminary 2-D shallow upper crustal tomographic velocity image was obtained by Prasad et al. [2006] showing the presence of alternate horst and grabens with high $V_p$ and $V_s$ of exhumed rocks. The model was constrained to 8 km depth only and do not answer about the origin of the presence of exhumation along with other deep seated geological structures. To address all these problems, 2-D tomographic imaging of both P-wave seismic refraction and wide-angle reflection data were used to derive a comprehensive geological model with internal P-wave velocity variations down to the Moho and configured the details about the zone of exhumation. The tomographic image obtained is further corroborated by Bouguer gravity modeling along the profile. The main objective of the study is to derive a comprehensive tectonic model of the crust toward south of SGT from wide-angle seismic, gravity, heat flux, geochemical and geochronological information etc., to understand the geodynamic setup of this region.

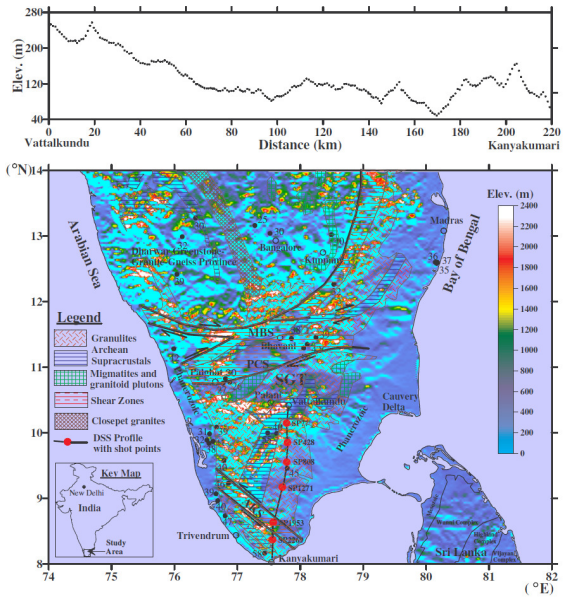


Figure 1: The geologic map of SGT showing exposures of different rock types superimposed with topography. The deep seismic sounding (DSS) profile from Vattalkundu to Kanyakumari is shown as solid line with SP's marked as red dots with respective numbers. The heat flux values (mW/m$^2$) are indicated as black dots at different places in the study region. The major shear zones are shown as PCS and AKS. The top panel represents the elevations along the said profile.

**Data quality and methodology**

The DSS profile toward south of SGT traverses across different shear and tectonically disturbed zones (Figure 1). The profile is relatively crooked with considerable topographic relief. Different SP gathers along the profile were prepared by applying crooked line geometry with elevation corrections (by using ProMax seismic data processing software) for each receiver station. These corrections make the receivers almost straight with respect to the SP and the picking error due to profile bending and elevations become negligible. The signal to noise ratio (SNR) of the P-wave data is good as shown from example record sections (Figure 2). The refracted and wide-angle reflected phases from different layer boundaries are picked manually for modeling/inversion. The sampling interval is 4ms and 5-10 Hz band-pass filtering is applied to the data.

The refraction phase through the crystalline crust ($P_g$) is observed for all the SP's. The pattern of the $P_g$ arrival varies significantly indicating a strong lateral variation in crustal structure along this transect. The reflection phase from the crust-mantle (Moho) boundary ($P_mP$) and intra-crustal boundaries ($P_iP$) are observed for five wide angle SP's with variable quality. Only those phases, which are coherent and correlated for long distances confirmed from the reciprocity tests of different source-receiver pairs are used for modeling.

The uncertainties and fitting of data play an important role in modeling. We have assigned picking uncertainties of 25 ms to the first-arrival refracted phases and 50 ms for reflected phases based on the criteria of 50% and 100% of the dominant period (e.g., 50 ms) as used by Behera et al. [2004] to avoid over and under fitting. The travel time fit and computation of synthetic seismograms [Zelt and Ellis, 1988] from the derived model along with the phase correlations of observed and theoretical ones are displayed in Figure 2 as an example. As a whole the travel time picks consists of 1073 direct arrivals, 5292 refracted phase ($P_g$), 14,236 reflected phases of $P_iP$ and $P_mP$ indicated as $P^1$ to $P^4$ (Table 1) for all the six SP's used for modeling/inversion. $P_n$ phase could not be recorded due to logistic problems.

**Table 1**: Crustal modeling results along Vattalkundu-Kanyakumari DSS profile

| Phases | No. of data picked | Picking uncert., ms | RMS resd., s | Norm. $\chi^2$ | No. of rays traced |
|---|---|---|---|---|---|
| $P_{direct}$ | 1073 | 25 | 0.011 | 0.204 | 1073 |
| $P_g$ | 5292 | 25 | 0.026 | 1.045 | 5290 |
| $P^1$ | 4000 | 50 | 0.025 | 0.256 | 3998 |
| $P^2$ | 4077 | 50 | 0.083 | 2.752 | 4076 |
| $P^3$ | 3365 | 50 | 0.037 | 0.546 | 3365 |
| $P^4$ | 2794 | 50 | 0.051 | 1.021 | 2792 |

**Initial model**

We have derived 1-D velocity-depth functions below each wide-angle SP's using the damped-least squares inversion technique in a layer-stripping fashion and the corresponding pseudo 2-D velocity model by smoothly joining these 1-D velocity-depth functions as illustrated in Behera et al. [2004]. The pseudo 2-D velocity model serves as a very good starting model for 2-D inversion to derive the preferred velocity model [Zelt, 1999; Zelt and Smith, 1992]. The velocity and depth uncertainties are chosen in order to obtain high parameter resolution and ability of the derived model to trace rays for all observed data points during inversion. The total number of data points used for inversion is 20,601 and rays traced for almost all data points through the model. The overall root mean square (RMS) travel time residual is 0.047 s and the normalized chi-square ($\chi^2$) value of 1.102 associated with various phases corresponding to all SP's along the profile is shown in Table 1.

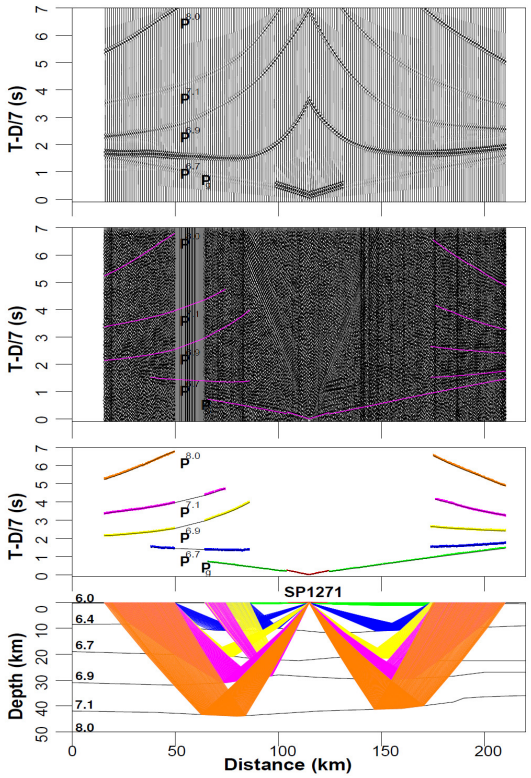


Figure 2: Two-dimensional ray trace modeling with travel time fit for SP1271 is shown along with corresponding observed and synthetics for the entire data. The picked (vertical bars) and predicted (solid lines) travel times for all the phases like $P_g$, $P_iP$ ($P^{6.7,\ 6.9,\ 7.1}$) and $P_mP$ ($P^{8.0}$) etc., are displayed with their corresponding travel time fit. For clarity every fifth traces are shown and all the data are plotted in reduced scale with a reduction velocity of 7.0 km/s.

## Preferred model

The final preferred velocity model derived is shown in Figure 3a. The upper crustal layers show velocities of 6.0 - 6.4 km/s and extend down to maximum 10 km depth. The mid-crustal layers have velocities of 6.7 km/s and 6.9 km/s with large intra-crustal undulations. The lower crust has 7.1 km/s velocity and Moho depth varies from 36-44 km having significant upwarping toward southern end of the profile. Since $P_n$ is not recorded, the constraints on the upper mantle velocity could not be established. However, 8.0 km/s is presumed for the upper mantle velocity as inferred from receiver function and DSS studies in the SGT [Rai et al., 2003; Reddy et al., 2003]. The preferred velocity model could not able to image any shallow and deep ctustal anomalous velocity variations and hence a more powerful tomographic inversion is adopted to resolve these features.

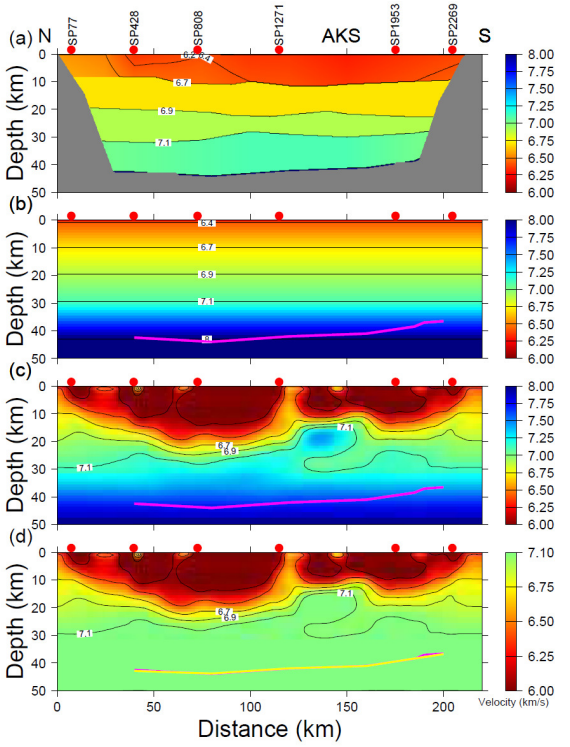


Figure 3: The final velocity model derived toward the south of SGT from inversion and tomography. (a) Preferred velocity model. (b) 1-D starting velocity model for tomography obtained from preferred model. (c) Final tomographic velocity image derived from refraction tomography. (d) Final velocity image obtained from reflection tomography with the Moho shown by bold yellow line. Bold pink line in Figures (b) – (d) represents the preferred Moho. The regions not sampled by rays in preferred model are left blank. The AKS zone, SP locations (red dots) and the color scale with contours indicates the velocity variations for each model.

**Seismic refraction and reflection tomography**

The first-arrival seismic refraction tomography adopted here is based on the algorithm of Zelt and Barton [1998]. For forward calculation, the model is parameterized using a uniform grid of velocity nodes. For inverse steps, the model is divided into rectangular cells of constant-slowness. The first-arrival travel times are calculated at each receiver locations by using the finite-difference eikonal solver of Vidale [1988], with modifications to handle large velocity contrasts by Hole and Zelt [1995]. A laterally homogeneous best-fit 1-D starting velocity model (Figure 4b) derived from the preferred model (Figure 4a) is used for tomographic inversion. The model is updated iteratively in which new ray paths are computed at each iteration until the satisfactory fit of observed travel times and the computed responses are obtained with $\chi^2$ of unity. For this date set, node spacing of 1.0 km is used, resulting 221 nodes across the length of the model. The cell-based model parameterization in the inverse step is controlled by rectangular cells having dimensions of 2.0 × 1.0 km for inverse grids. We have obtained the final image after eight non-linear tomographic inversions, dropping the RMS travel time misfits from starting to the final model by a factor of six. The tomographic image is very smooth (Figure 3c) showing all the structural elements and lateral heterogeneities, which could not be deciphered in the preferred velocity model (Figure 3a).

For the reflection tomography, we have employed the same algorithm of Zelt and Barton [1998] with the exception that only one reflected phase ($P_mP$) and one interface (the Moho) is used while fixing the velocity model. The Moho is parameterized uniformly for both forward and inverse steps using node spacing equal to the forward velocity grid nodes. The reflection travel times are calculated using a finite-difference solution to the eikonal equation. The starting model used for this is flat. The model updates are determined iteratively in which new ray paths are calculated at each iteration, until the observed $P_mP$ travel times are predicted by the model with $\chi^2$ value close to one. The inversion of the first arrivals and $P_mP$ were decoupled in the same way as described by Zelt et al. [2003], using the former to solve for the velocity model and the later only for the Moho geometry keeping the velocity field fixed. Similar to the refraction tomography, the main aim of reflection tomography is to derive the most featureless model that fits the reflection travel times ($P_mP$) from the Moho boundary (Figure 3d).

**Model assessment**

The perturbation of the final tomographic velocity image with respect to the starting model is shown in Figure 4a, which reveals very crucial information like the truncation of fault blocks in the shallow upper crust. The length-scales of the perturbations are a function of the resolution provided by the data, and hence the real subsurface structure. The perturbations reach a maximum value of 0.75 km/s in magnitude. An anomalous large positive velocity perturbations of >0.4 km/s lies beneath the AKS zone at 20 – 30 km depth range may be considered as the probable zone of the source of exhumation. The tomographic image is also further constrained by ray cell hit counts (Hits) along the transect (Figure 4b). The poor ray coverage is indicated by fewer hits in deeper part of the model. The hits are a measure of the number of rays sampling each cell of the model. To assess the lateral resolution of the model, we have performed checkerboard resolution test [Zelt and Barton, 1998] having 25 × 5 km cell size with ±0.5 km/s perturbations with respect to the preferred model. The alternate positive and negative anomaly pattern extends from 0.0 km depth to the bottom of the model (50.0 km). The checkerboard test has the same source receiver geometry of the real data picked. The data were inverted using the preferred starting model and same free parameters. An assessment of the recovered anomaly pattern (Figure 4c) indicates a measure of spatial resolution throughout the model (>0.25 km/s) having large lateral heterogeneity in the upper crust. The recovery of the tomographic image shown by alternate positive and negative checkers with good resolutions and the nature of velocity perturbations show a clear evidence of the presence of high velocity mafic granulites at this depth later exhumed to the surface through the shear zones.

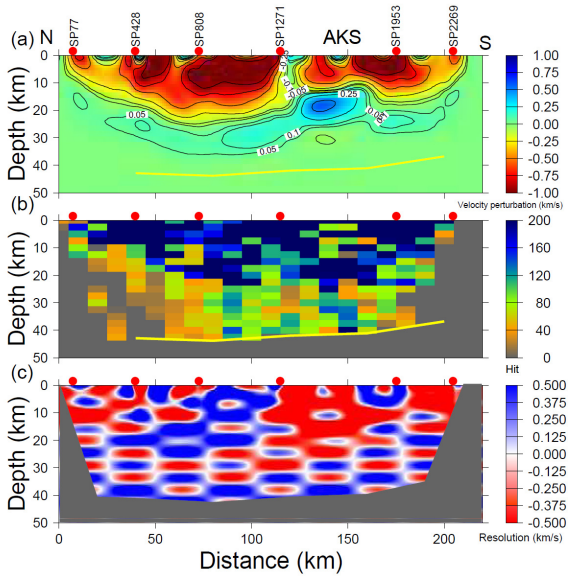


Figure 4: (a) Perturbation plot of the tomographic velocity model indicated by color scale with contours. Alternate positive and negative velocity perturbations represent horst and graben features imaged from the seismic tomography. (b) Ray hit count plot with hits shown in color scale. The Moho boundary obtained from reflection tomography is shown as thick yellow line. (c) Checkerboard resolution test showing very good recovery of the derived model having resolutions (>0.25) shown in the color scale.

## Crustal density modeling

The Bouguer gravity anomaly generally reflects density and thickness variations of the crust and upper mantle. The relationships between the seismic and gravity models are studied for a better understanding of the geology and tectonics of the region to constrain the model as per the geodynamic evolution. The model parameterization of Zelt and Smith [1992] has been adopted to compute the gravity responses utilizing the 2-D gravity modeling algorithm [Nielson and Jacobson, 2000; Talwani et al., 1959]. The Bouguer gravity data along the said DSS profile has been obtained at irregular intervals from the latest 5 mGal Bouguer gravity anomaly map [NGRI, 2006] to retain maximum gravity features in the data. The mean error or uncertainty associated with the observed gravity data is of the order 2.0 mGal. The nature of Bouguer gravity data along the profile show alternate lows and highs varying from -85 to -35 mGal (Figure 5). The gravity data indicates the presence of numerous shallow alternate horst and graben features with deep seated high density bodies in the mid-to-lower crustal level due to sharp rise of gravity values. To make the density model more comprehensive and corroborate shallow and deep crustal elements, we have tried to fit the gravity data by deriving a density model taking into account the same velocity and interface structures of the tomographic velocity image (Figure 3c).

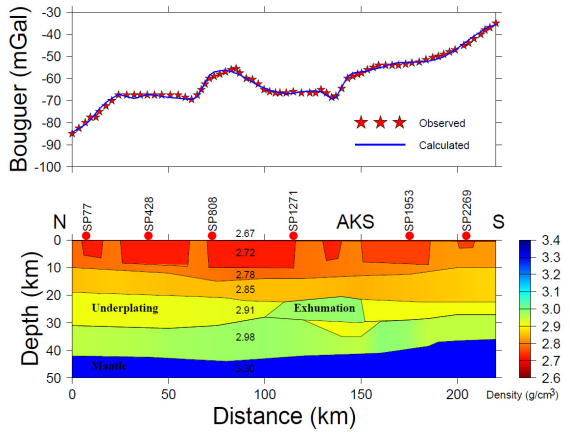


Figure 5: Observed (red stars) and computed (blue line) Bouguer gravity response (top panel) from the derived density model (bottom panel). The variation of density values for different layers are shown in the color scale along with the average density values indicated within the model.

We have used the method of Nielson and Jacobson [2000] for gravity inversion by taking into account the initial model derived from the tomography. We have used absolute densities derived from the velocity-density relationships for the gravity inversion as opposed to the density contrasts. The model parameters adjusted during the inversion are boundary depths and density values. The density values and the boundary depths within each block are adjusted automatically during inversion so that an optimum fit of the observed and computed response of Bouguer gravity anomaly with normalized $\chi^2$ value close to one (1.20) is obtained after ten iterations. The RMS residual of the observed and computed gravity response is of the order of 2.0 mGal. The final gravity model constrained from the tomographic velocity image along with the data fit is shown in Figure 5.

## Tectonic and geodynamic implications

A comprehensive tectonic model (Figure 6) is derived from this study of seismic tomography, Bouguer gravity, heat flux, geological/geochronological informations available in this segment of the SGT. The Bouguer gravity and heat flux values corroborate very well with the seismic tomography results, which vindicates the formation of a large suture as AKS zone during Pan-African rifting with collision tectonics. The presence of very thick (18 km) high average velocity (6.8 km/s) and density (2.88 g/cm$^3$) materials in the mid crustal level underlain by 10 km thick lower crust with velocity of 7.1 km/s and density of 2.98 g/cm$^3$ represents a typical collision environment and underplating. The crust is thinned toward south end of the profile showing significant Moho upwarping may be attributed to the upwelling of mantle materials (Figure 6). The presence of numerous shear zones like PCS, AKS etc., bolsters our findings of the high velocity and high density mafic materials considered as granulites in the mid to lower crustal level (20 - 30 km depth) from both seismic tomography and gravity modeling. The Moho structure is derived from both preferred and tomographic velocity models show very little deviations, hence well constrained. The new heat flux measurements in the south of SGT also indicate highest value so far observed in the entire granulite-gneiss province of south India (~58 mW/m$^2$) [Roy et al., 2007]. This strengthens our findings of the source region of the mafic granulites near AKS zone. The geodynamic evolution of this region is very complex, although with the help of the limited data set available, we can infer that high velocity (>7.0 km/s) and high density (>2.95 g/cm$^3$) mafic materials have intruded through the conduits, exhumed in mid-to-lower crustal level and later deposited on the surface through major shear zones (Figure 6) following large scale intracontinental collision and shearing process due to Pan-African tectonic activity.

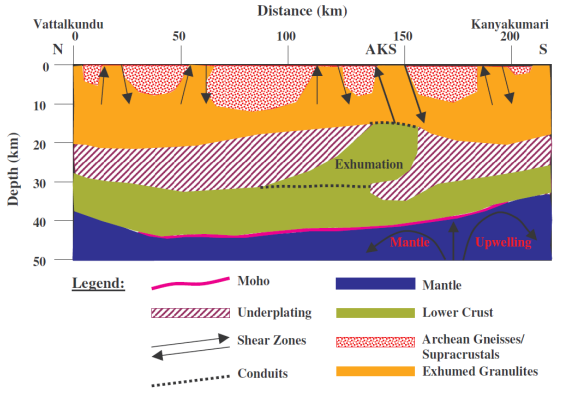


Figure 6: The comprehensive tectonic and geodynamic model toward south of SGT derived from combined tomographic and gravity modeling. The various crustal elements imaged are alternate horst and grabens in the upper crust, thick underplated region with significant Moho upwarping and upwelling of the mantle materials. The source region of exhumed mafic granulites in the mid to lower crust below the major shear (AKS) is displayed toward south of SGT.

## Conclusions

The preferred velocity model derived is considered as geologically plausible but lacks in imaging the complex geological features both at shallow and deeper levels. Since this region is tectonically disturbed with numerous shear zones, which are not apparent in the preferred model, we have tried to image this region with more powerful tomographic imaging technique by using seismic refraction and wide-angle reflection data. The tomographic image is also further corroborated by gravity inversion to develop a comprehensive geodynamic model toward south of SGT (Figure 6) showing alternate horsts and grabens with shear zones like AKS, source of exhumation of mafic granulites, underplating in the mid-to-lower crustal level followed by Moho upwarping and mantle upwelling. This comprehensive model deciphers most of the geological features for better understanding of the complex geodynamic processes involved in the formation and evolution of south of SGT taken place during the Pan-African tectonothermal activity.

**Acknowledgments**

We are grateful to V. P. Dimri, Director, NGRI for according permission to publish this paper. We also gratefully acknowledge the Department of Science and Technology (DST), Govt. of India for funding and the Controlled Source Seismic Project (CSSP) team members for necessary support to acquire DSS data in the SGT, India.

**References**

Behera, L., Sain, K. and Reddy, P. R., 2004, Evidence of underplating from seismic and gravity studies in the Mahanadi delta of eastern India and its tectonic significance; J. Geophys. Res., 109, B12311, doi:10.1029/2003JB002764, 1-25.

Guru Rajesh, K. and Chetty, T. R. K., 2006, Structure and tectonics of the Achankovil Sear Zone, southern India; Gondwana Research, 10, doi:10.1016/j.gr.2005.11.018, 86-98.

Hole, J. A. and Zelt, B. C., 1995, Three-dimensional finite-difference reflection travel times, Geophys. J. Int., 121, 427-434.

National Geophysical Research Institute (NGRI), 2006, Gravity map series of India, scale 1:2,000,000, Hyderabad, India.

Nielsen, L. and Jacobson, B. H., 2000, Integrated gravity and wide-angle seismic inversion for tow-dimensional crustal modeling, Geophys. J. Int., 140, 222-232.

Percival, J. A. and Card, K. D., 1983, Archean crust as revealed in the Kapuskasing uplift, Superior Province, Canada; Geology, 11, 323-326.

Prasad, B. R. Behera, L., and Rao, P. K., 2006, A tomographic image of upper crustal structure using P and S wave seismic refraction data in the southern granulite terrain (SGT), India; Geophy. Res. Lett., 33, L14301, doi:10.1029/2006GL026307, 1-5.

Rai, S. S., Priestley, K., Suryaprakasam, K., Srinagesh, D., Gaur, V. K. and Du, Z., 2003, Crustal shear velocity structure of the south Indian shield, J. Geophys. Res., 108, B2, 2088, doi:10.1029/2002JB001776, ESE 10, 1-12.

Ramakrishna, M., 2003, Tectonics of southern granulite terrain; Mem. Geol. Soc., India, 50, 1-434.

Reddy, P. R., Prasad, B. R., Rao, V. V., Sain, K., Rao, P. P., Khare, P. and M. S. Reddy, M. S., 2003, Deep seismic reflection and refraction/wide-angle reflection studies along Kuppam-Palani transect in the southern granulite terrain of India, Mem. Geol. Soc. India, 50, 79-106.

Roy, S., Ray, L., Bhattacharya, A. and Srinivasan, R., 2007, New heat flow data from deep boreholes in the greenstone granite-gneiss and gneiss-granulite provinces of south India, DCS-DST Newsletter, 17, 1, 8-11.

Talwani, M., Worzel, J. L. and Landisman, M., 1959, Rapid gravity computations for two-dimensional bodies with application to the Mendocino submarine fracture zone, J. Geophys. Res., 64, 49-59.

Vidale, J. E., 1988, Finite-difference calculation of travel times, Bull. Seism. Soc. Am., 78, 2062-2076.

Zelt, C. A., 1999, Modeling strategies and model assessment for wide-angle seismic travel time data; Geophys. J. Int., 139, 183-204.

Zelt, C. A. and Barton, P. J., 1998, Three-dimensional seismic refraction tomography: A comparison of two methods applied to data from Faroe Basin, J. Geophys. Res., 103, 7187-7210.

Zelt, C. A. and Ellis, R. M., 1988, Practical and efficient ray tracing in two-dimensional media for rapid travel time and amplitude forward modeling, Can. J. Explor. Geophys., 24, 16-31.

Zelt, C. A., Sain, K., Naumenko, J. V. and Sawyer, D. S., 2003, Assessment of crustal velocity models using seismic refraction and reflection tomography, Geophys. J. Int., 153, 609-626.

Zelt, C. A. and Smith, R. B., 1992, Seismic travel time inversion for 2-D crustal velocity structure, Geophys. J. Int., 108, 16-34.